

Electronic voltage control of magnetic anisotropy at room temperature in high- κ SrTiO₃/Co/Pt trilayer


Bart F. Vermeulen^{1,*}, Johan Swerts,² Sébastien Couet,² Mihaela Popovici,² Iuliana P. Radu,² Joris Van de Vondel³, Kristiaan Temst³, Guido Groeseneken,^{4,†} and Koen Martens^{1,†}

¹Laboratory for Semiconductor Physics, KU Leuven, Leuven, Belgium

²IMEC, Kapeldreef 75, Leuven, Belgium

³Quantum Solid-State Physics, Department of Physics and Astronomy, KU Leuven, Celestijnenlaan 200D, Leuven, Belgium

⁴Department of Electrical Engineering, KU Leuven, Leuven, Belgium

 (Received 20 April 2020; revised 7 September 2020; accepted 22 October 2020; published 19 November 2020)

To improve power efficiency and endurance of magnetic memory technologies, a voltage-controlled mechanism is desirable. The voltage control of magnetic anisotropy (VCMA) effect in MgO stacks is a promising option, however, its strength is too low for memory applications. Replacing the standard MgO layer by an oxide with a higher permittivity κ may help improve the VCMA strength. We demonstrate a VCMA effect up to $\xi = 75$ fJ/Vm at room temperature in a Co/Pt bilayer grown on atomic layer deposited (ALD) high- κ SrTiO₃ (STO). After treating the STO surface with isopropanol, a thin CoO_x interfacial layer is observed, enabling VCMA. Upon cooling down from room temperature to 200 K, the VCMA effect strength increases by a factor of two. This increase is incompatible with the expected Arrhenius temperature dependence for an ionic effect and thus we argue that the observed VCMA effect is electronic. Electronic VCMA is desirable for adequate memory endurance, and hence the approach proposed here has great potential for applications.

DOI: [10.1103/PhysRevMaterials.4.114415](https://doi.org/10.1103/PhysRevMaterials.4.114415)

I. INTRODUCTION

Voltage control of the magnetic anisotropy (VCMA) of ferromagnetic metals can enable the next generation of low power magnetic random access memory (MRAM) technologies. Using a voltage-based switching scheme, the MRAM switching energy can be decreased from 100 fJ/bit [1] down to 6 fJ/bit [2,3]. The VCMA effect [4,5] may be used in the next generation of MRAM devices to decrease the energy barrier for information retention and hence strongly reduce the switching energy. In order to completely remove this energy barrier, a VCMA effect with a strength of $\xi = 1000$ fJ/Vm [6,7] is desirable.

In VCMA [4], an electric field is applied across a dielectric/ferromagnet interface. Charge accumulation at this interface leads to a modulation of interfacial orbital magnetic moments [5,8] and interfacial electric quadrupoles [5,9]. Both mechanisms lead to a modification of the interfacial anisotropy energy [5]. VCMA is mostly obtained using MgO as a dielectric, and MRAM-compatible ferromagnetic layers such as Fe [4,9–12], FeCo [13], Co_xFe_yB [14–17], and Co [18–23]. The deposition method has a decisive impact on the VCMA effect strength. Currently, a room temperature VCMA modulation coefficient $\xi = 100$ fJ/Vm has been reported in Ta/CoFeB/Mg/MgO sputter-deposited on thermally ox-

idized Si [24]; and up to $\xi = 370$ fJ/Vm on molecular beam epitaxy (MBE)-grown MgO(001)/MgO/Cr/Fe/MgO [11]. Unfortunately, experimental results using MgO rarely exceed $\xi = 50$ fJ/Vm. A method which substantially increases the strength of the VCMA effect is therefore needed.

Considering the charge-based nature of the VCMA effect [5], it is desirable to maximize the amount of accumulated interfacial charge. Replacing the MgO dielectric (with a relative permittivity $\kappa = 9.8$) with a high- κ dielectric increases the interfacial charge ΔQ per applied volt and may increase ξ :

$$\xi \propto \frac{\Delta Q}{A} = \epsilon_0 \kappa E \quad (1)$$

with ΔQ the charge, A the area of the capacitor, ϵ_0 the permittivity of vacuum and E the electric field across the oxide. Although this has been theoretically proposed before [15,17,21,25–27], there is little experimental work exploiting this concept. So far, a large VCMA effect of 230 fJ/Vm at room temperature on a high- κ dielectric has been reported using Pt/Co/CoO_x/HfO₂ [28].

High- κ dielectrics like SrTiO₃ can nowadays be grown on a large scale using atomic layer deposition (ALD). ALD growth is compatible with modern electronics applications, and it allows to grow STO with good (110) surface crystallinity [29,30], low leakage currents [30], and a dielectric constant up to 80 [29].

However, in ALD-grown high- κ layers such as STO, oxygen vacancies have been shown to impact the dielectric properties (such as permittivity) of the layer [31], and can contribute to the conductivity if they are mobile [32,33]. Large modulations of the magnetic anisotropy energy have

*Also at IMEC, Kapeldreef 75, Leuven, Belgium; bart.vermeulen@imec.be

†Also at IMEC, Kapeldreef 75, Leuven, Belgium; koen.martens@imec.be may

been achieved using oxygen ion migration in high- κ GdO_x , with a strength up to 11.6 pJ/Vm [34–36]. Even though the modulation coefficient on GdO_x is particularly large, the ionic effect is slow and offers poor long term stability for memory applications. For electronics applications, a purely electronic effect is desired, and it is crucial to ascertain that oxygen vacancies play no role in the VCMA effect measured in this work.

One method for differentiating the contribution of oxygen vacancies from electronic effects is to measure the temperature dependence of the VCMA effect. Indeed, the mobility of oxygen vacancies follows an Arrhenius law [32]. The kinetics of an ion-mediated effect freezes out at decreasing temperatures, which suppresses the modulation altogether. On the other hand, in STO single crystals\Co\Pt, the VCMA strength is claimed to increase exponentially from 1.3 pJ/Vm at 150 to 23.1 pJ/Vm at 2 K [21]. The authors ascribe the increase of the VCMA coefficient to the strong increase of the permittivity of single crystal STO [37]. However, the effect of thermal expansion coefficient mismatch (which is important in epitaxial stacks on single crystals, and has been shown to impact VCMA [38,39]) and the temperature effect on the ferromagnet band structure were not taken into account. Finally, single-crystal substrates other than silicon are not compatible with microelectronics applications.

In our recent work, we have shown that perpendicular magnetic anisotropy (PMA) can be obtained in a ferromagnetic film deposited on ALD-grown oxides like amorphous (a-)HfO₂ [40,41]. However, no VCMA was detected. The lack of VCMA was ascribed to the thick magnetic dead layer (MDL, $t_{\text{MDL}} = 0.53$ nm [40]) at the a-HfO₂\ferromagnet interface. To improve the quality of the oxide\ferromagnet interface and minimize t_{MDL} , the aim of this paper is to investigate crystalline SrTiO₃, and to apply surface cleaning treatments prior to the deposition of the ferromagnetic layer. Here, a VCMA effect in STO\Co(Pt)\Pt is reported with a strength up to $\xi = 75$ fJ/Vm. Furthermore, from the temperature dependence of the VCMA effect, we conclude that it is highly unlikely that a mechanism based on oxygen vacancies, oxygen ions, redox reactions or other chemical processes is at play. Instead, the VCMA effect in this system is electronic.

II. MATERIALS BULK AND INTERFACIAL PROPERTIES

In this section, we discuss the material properties of the STO\Co(Pt)\Pt samples. First, the structural properties are investigated with transmission electron microscopy (TEM). Second, we mention the importance of the thin CoO_x layer at the STO\Co interface (the characterization of the interface is discussed at length in the supplementary information [42]). Finally, the magnetic properties of the samples are discussed.

A. Structural properties and layer thicknesses

The thickness and crystallinity of the layers is investigated using transmission electron microscopy [TEM, see Fig. 1(a)]. The ALD STO layer is 10.1 ± 0.5 nm thick, and it consists of crystalline grains with the thickness of the layer. The underlying TiN template layer has a thickness of 9.1 ± 0.5 nm. The Pt and Co layers have a combined thickness of 4.9 ± 0.5 nm;

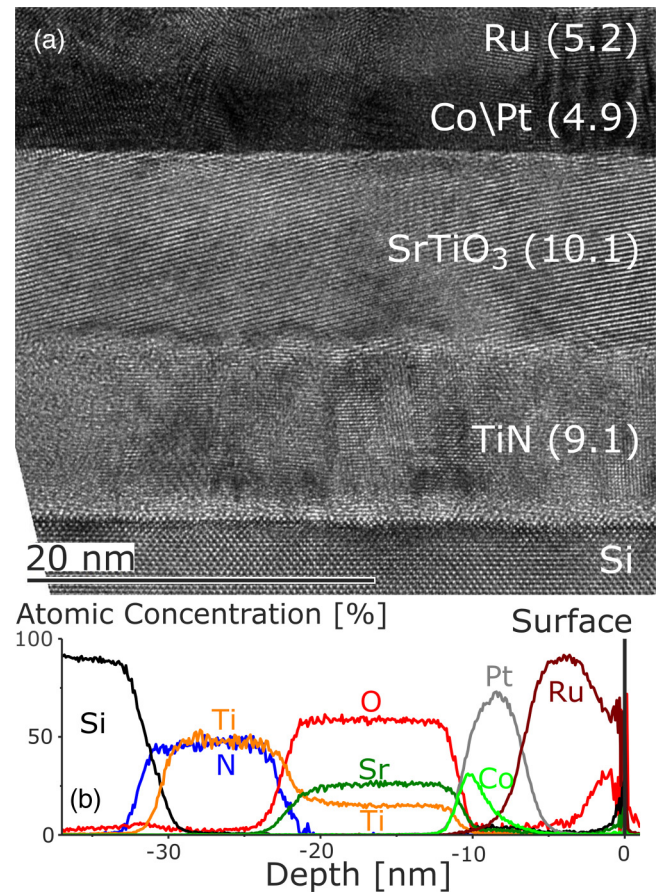


FIG. 1. (a) Transmission electron microscopy (TEM) image of a sample on the Co thickness wedge location with $t_{\text{Co}} = 0.8$ nm. The layer thickness in nm is indicated between parentheses. (b) Energy-dispersive x-ray spectroscopy (EDS) image shows the Co/Pt interdiffusion.

they cannot be distinguished due to interdiffusion [40,43]. This interdiffusion is clearly visible in the energy-dispersive x-ray spectroscopy (EDS) measurement of Fig. 1(b). Given the Co-Pt interdiffusion during anneal, the magnetic stack consists of a CoPt\Pt bilayer rather than the as-deposited Co\Pt bilayer. Besides leading to the interdiffusion of Co and Pt, the annealing treatment also leads to recrystallization of the Co layer into the fcc (111) phase [40,43].

Finally, the cobalt layer is deposited with a thickness wedge along the diameter of the wafer, ranging from $t_{\text{Co}} = 0.6$ to 2.4 nm (measured using Rutherford backscattering spectroscopy).

B. STO\Co interfacial oxidation

To improve the quality of the STO\Co interface and promote VCMA, a thin CoO_x layer is desirable. The thin CoO_x interface layer is formed after an STO surface treatment using isopropanol. The interfacial CoO_x layer promotes uniform magnetization switching, which results in a square hysteresis loop with full remanence [see Fig. 2(a)] and is necessary for observing VCMA [44]. The motivation for obtaining a CoO_x layer and the characterization of the STO\Co interface with x-ray photoelectron spectroscopy (XPS) are explained at length in Secs. SI.a through SI.e of Ref. [42] and Refs. [45–53].

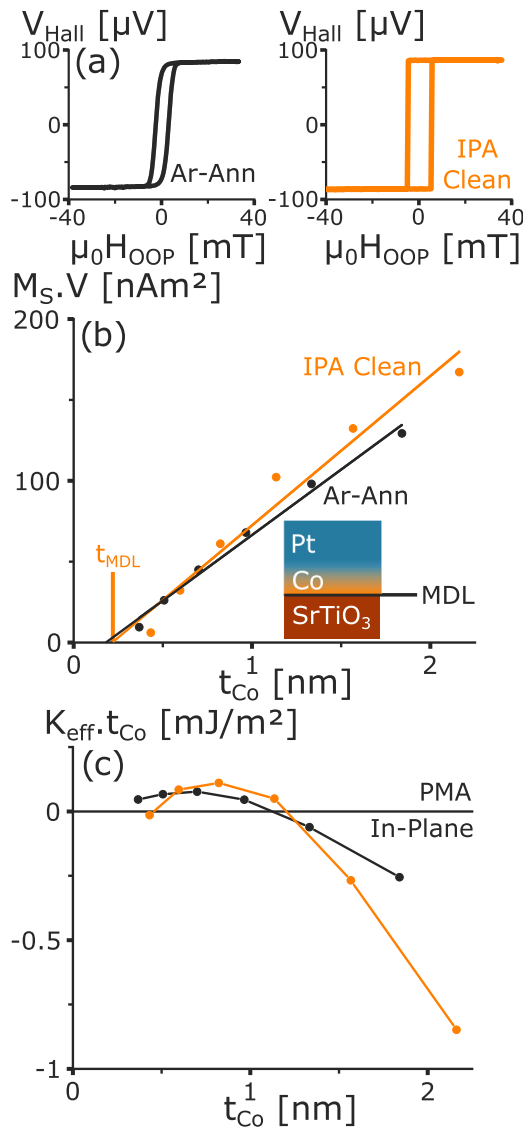


FIG. 2. (a) The out-of-plane (OOP) magnetic hysteresis loop measured with the anomalous Hall effect for both samples. (b) The magnetic moment $M_S V$ and (c) the effective anisotropy energy $K_{\text{eff}} t_{\text{Co}}$ vs cobalt thickness t_{Co} for $8 \times 8 \text{ nm}^2$ samples cleaned in IPA and samples with Ar⁺ ion milling + 350 °C UHV anneal.

In the next section, the magnetic properties of samples with CoO_x and without CoO_x interface layer are discussed. They are obtained using the following two surface treatments: (1) IPA (CoO_x interlayer): an isopropanol (IPA) clean; and (2) Ar-Ann (no CoO_x): Ar⁺ ion milling followed by an *in situ* UHV anneal at 350 °C.

C. Magnetic properties

The magnetic properties of samples Ar-Ann and IPA are investigated using VSM. The magnetic moment $M_S V$ (with V the volume of the ferromagnetic layer) and the effective anisotropy energy $K_{\text{eff}} t_{\text{Co}}$ are measured as a function of the cobalt thickness t_{Co} and the STO surface treatment (see Fig. 2). From $M_S \cdot V$ and $K_{\text{eff}} \cdot t_{\text{Co}}$ the magnetization M_S , the thickness of the magnetic dead layer t_{MDL} , the interfacial

TABLE I. The magnetic properties of samples Ar-Ann and IPA.

Parameter	Ar-Ann	IPA Clean
M_S (MA/m)	1.28 ± 0.06	1.50 ± 0.14
t_{MDL} (nm)	0.19 ± 0.05	0.25 ± 0.11
K_i (mJ/m ²)	0.33 ± 0.03	0.86 ± 0.04
$-K_V$ (MJ/m ³)*	0.35	0.89

*The standard deviation is below 0.0001.

anisotropy energy K_i and the volume anisotropy energy K_V are calculated (see Table I).

The magnetic dead layer is thicker in the sample cleaned with IPA ($t_{\text{MDL}} = 0.25 \pm 0.11 \text{ nm}$) than in the ion-milled + annealed sample ($t_{\text{MDL}} = 0.19 \pm 0.05 \text{ nm}$), although the difference is within the error margin. The layer of CoO_x is expected to consume some interfacial cobalt atoms [54]. CoO_x is not ferromagnetic, and is not expected to contribute to the magnetic moment, hence the thicker MDL.

In previous work [40,41], we argued for reducing the magnetic dead layer thickness to allow a measurable VCMA effect. The thickness of an atomic monolayer of Co fcc (111), for example, is 0.205 nm [55]. Given that t_{MDL} is of the order of the thickness of a single atom layer, the small difference between samples Ar-Ann and IPA is likely ascribed to a slightly increased roughness of the MDL. Furthermore, the MDL thickness is in both cases well below the value reported on amorphous HfO_2 (where $t_{\text{MDL}} = 0.53 \text{ nm}$ [40]). The interfacial anisotropy energy K_i is more than double for the IPA-cleaned sample (see Table I). The additional oxygen at the interface is indeed expected to improve the PMA through hybridization with the Co 3d orbitals [56,57]. Interfacial PMA can reach a maximum as a function of the degree of oxidation of the interface [54,58]. Here, it seems that for the IPA-cleaned sample with a $K_i = 0.86 \pm 0.04 \text{ mJ/m}^2$, the STO/Co interface contributes strongly to the anisotropy. The contribution of the STO/Co surface is around $0.3 \pm 0.05 \text{ mJ/m}^2$; it corresponds to the difference between the measured K_i and the expected contribution of the Co/Pt interface (0.55 mJ/m^2 [55,59,60]).

The magnetization is larger for the IPA-cleaned sample as well, which may indicate that there is a larger degree of interdiffusion-driven proximity-induced magnetization of the Pt layer [40,61,62]. The volume anisotropy $-K_V$ originates from three contributions, the dipolar anisotropy K_D , the magnetocrystalline anisotropy K_{mc} and the strain anisotropy K_{ms} . The dipolar anisotropy is equal to $K_D = -\frac{\mu_0 M_S^2}{2}$. So an increase of the magnetization of 17% can account for a 37% larger K_V through the increase in K_D . However, the K_V is 2.5 times larger for the sample cleaned with IPA, which has to be due to the higher K_{mc} or K_{ms} . It is likely that the lower K_V of the Ar⁺ ion milled sample is due to the same reason as the lower M_S , i.e., the damaged, amorphized surface of STO leads to a Co(Pt) layer with degraded crystallinity. The magnetization suffers from this lower crystallinity and so does the magnetocrystalline contribution to K_V .

In summary, inspite of the thicker MDL present at the STO/Co interface following the IPA Clean treatment, those samples show higher magnetization, interfacial and volume anisotropy. Furthermore and most importantly, the IPA Clean treatment promotes uniform magnetization switching.

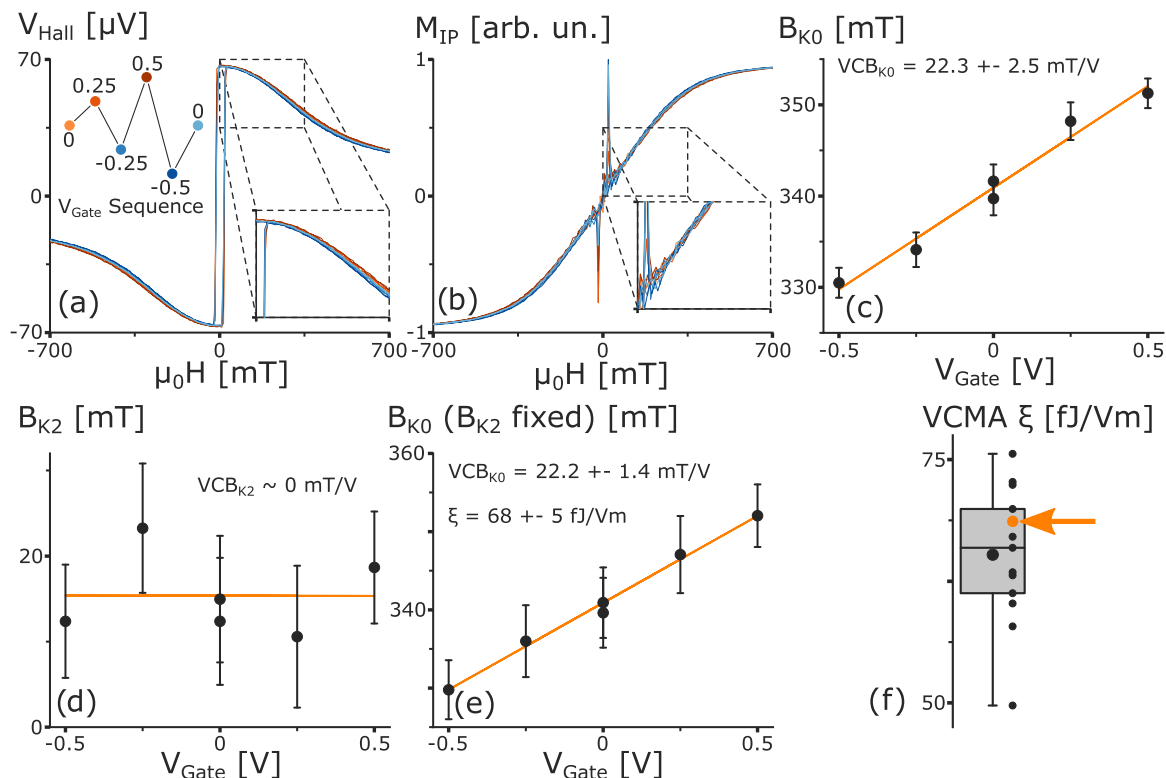


FIG. 3. The VCMA effect in STO/Co(Pt)/Pt for IPA cleaned samples with $t_{\text{Co}} = 0.66$ nm with $\theta_H = 82^\circ$. (a) AHE measurement as a function of the in-plane field. The upper left inset shows the sequence of gate voltages. (b) The calculated in-plane component of the magnetic moment. The dependence of (c) B_{K0} and (d) B_{K2} on V_{Gate} across STO. (e) The dependence of B_{K0} on V_{Gate} when B_{K2} is held constant at $B_{K2}(V_{\text{Gate}} = 0\text{V})$. (f) The amplitude of the VCMA effect (with B_{K2} fixed) in samples with $t_{\text{Co}} = 0.66$ nm. The arrow indicates the sample shown in (a)–(e). The sign of VCMA is defined as positive when accumulation of electrons in the ferromagnetic layer leads to an increase in the anisotropy energy.

III. VCMA IN STO/Co(Pt)/Pt

This section and the remainder of this publication describe the VCMA effect in sample IPA, with uniform magnetization switching. The Co thickness $t_{\text{Co}} = 0.66$ nm. Sample Ar-Ann also shows a modulation of the hysteresis loop as a function of the gate voltage V_{Gate} , however, it is discussed in Sec. SII in Ref. [42]. Quantifying VCMA using AHE measurements is not as straightforward as one would expect. In Sec. SIII [42] and Refs. [23,63–71], we first discuss our measurement methodology, and a commonly used model for analyzing the data (the Ellipse Model, see Sec. SIII.A), which arises from a basic understanding of magnetic anisotropy. This model is used to quantify VCMA in our samples (see Sec. SIII.B), but contains several fundamental shortcomings (see Sec. SIII.C) and ultimately is not reliable for quantifying VCMA. Instead, we quantify the VCMA effect using the Sucksmith-Thompson (ST) model [72] (derived in Sec. SIII.D). The ST model describes the path of the magnetic moment in function of the applied magnetic field and the anisotropy fields, and is expressed as follows:

$$B_{K0} + B_{K2} \sin^2 \theta_M = \mu_0 \|H_{\text{ext}}\| \left(\frac{\cos \theta_H}{\cos \theta_M} - \frac{\sin \theta_H}{\sin \theta_M} \right) \quad (2)$$

where $B_{K0,K2}$ represent the zeroth, respectively second order anisotropy fields, $\theta_M = \arccos(V_{\text{Hall}}/V_{\text{Hall,Sat}})$ is the angle of the magnetic moment, θ_H is the angle of the field, and $\mu_0 \|H_{\text{ext}}\|$

is the applied magnetic field. Hence, from the magnetic-field dependence of θ_M , the anisotropy fields can be derived. The ST model is a valuable tool to separate the zeroth-order anisotropy field B_{K0} from the second order anisotropy field B_{K2} [73].

The effect of the gating voltage on the AHE measurement is shown in Figs. 3(a) and 3(b). The zeroth and second order magnetic anisotropy fields $B_{K0,K2}$ from Eq. (2) are shown in Figs. 3(c) and 3(d). Before quantifying the VCMA effect in this sample [from B_{K0} , see Figs. 3(c)], the gate voltage-dependence of B_{K2} [see Fig. 3(d)] is investigated. The second order magnetic anisotropy is not impacted by the gate voltage, whereas the zeroth order anisotropy is strongly impacted. B_{K2} likely originates from the remaining impurities that have not been removed by the IPA clean (see Sec. SIII.E [42]). One could hypothesize that the magnetic properties of these impurities may be impacted by the gating voltage, and lead to an effect on the magnetic properties of the Co(Pt) related to these impurities i.e. B_{K2} . However, there is no modulation of B_{K2} in this sample. The modulation of B_{K2} has been demonstrated using piezoelectric strain [74], but in publications that attempt to measure the modulation of B_{K2} through VCMA, no voltage control of B_{K2} is observed [75–77].

Since B_{K2} is not modulated by V_G , instead of fitting the ST model (2) with both B_{K0} and B_{K2} function of V_G , B_{K2} is fixed at the value of B_{K2} for $V_{\text{Gate}} = 0\text{V}$. The result with this simplified fitting algorithm is shown in Fig. 3(e). Using

TABLE II. Comparison of the VCMA effect models using a dataset for $t_{\text{Co}} = 0.66$ nm.

Model	VCB_{K0} (mT/V)	B_{K0} (mT)
Sucksmith-Thompson (ST)	22.3 ± 2.5	340.9 ± 0.8
ST (B_{K2} fixed)	22.2 ± 1.4	340.9 ± 0.5

the fitting procedure with fixed B_{K2} improves the linearity of the fitting. Both B_{K0} and its voltage modulation VCB_{K0} remain the same (see Table II). However, the standard deviation for both parameters decreases by 40%. The fact that the fitting linearity improves when a parameter is held constant is counter intuitive, and is an indication that B_{K0} and B_{K2} are correlated to some extent. This correlation stems from the fact that, in samples with some nonuniformities, B_{K2} is not to be interpreted as an anisotropy field but is related to the remaining nonuniformities in the samples (see earlier and Sec. III E [42]). This shortcoming of the ST model illustrates the challenges of measuring the VCMA effect using transport measurement methods, and the importance of achieving uniform magnetization switching for measuring VCMA. The amplitude of the VCMA effect ξ in Fig. 3(f) is calculated from VCB_{K0} as follows:

$$\xi \left[\frac{\text{J}}{\text{V m}} \right] = \frac{1}{2} VCB_{K0} M_S (t_{\text{Co}} - t_{\text{MDL}}) t_{\text{STO}}, \quad (3)$$

where M_S is the magnetization, t_{Co} , t_{MDL} and t_{STO} the cobalt, MDL and STO thicknesses respectively (from Table I). The VCMA effect in STO\Co(Pt)\Pt with $t_{\text{Co}} = 0.66$ nm measured on different devices ranges from 50 ± 6 to 75 ± 8 fJ/Vm. The average VCMA effect strength is 65 ± 6.5 fJ/Vm [see distribution in Fig. 3(f)].

The VCMA effect strength reported for cobalt ranges from negative 147 fJ/Vm to positive 230 fJ/Vm (see Table III for an overview of the literature). Positive (negative) VCMA refers to an increase (decrease) of the effective anisotropy energy upon accumulation of electrons at the oxide/ferromagnet interface. Small differences in the strain state or interfacial contamination have a dramatic effect on the amplitude and even sign of VCMA. Recently, VCMA with a strength of 230 fJ/Vm was reported in Pt\Co\CoO_x\HfO₂ layers [28]. The authors show that the VCMA effect is stronger when a CoO_x layer is added at the Co\HfO₂ interface, which

TABLE III. The VCMA effect in cobalt in literature.

Material	ξ (fJ/V m)	Reference	Year
MgO\Co\Pt	+32*	[18]	2013
V\Fe\Co\MgO	-82	[19]	2017
Pt\Co\MgO	-147	[20]	2017
Pt\Co\MgO	2.5	[22]	2018
Pt\Co\CoO _x \HfO ₂	+230	[28]	2018
Ta\Pt\Co\MgO	-40*	[23]	2019
Ta\Pt\Co\Pt\Co\MgO	-77*	[23]	2019

*The VCMA effect is not explicitly quantified, the number reported here is calculated based on numerical data/graphs available in the publication.

had already been shown before for voltage control of the coercivity [78]. Together with the results presented in this work, the importance of a proper degree of oxidation of the oxide/ferromagnet interface becomes clear. Interfacial oxygen has a strong impact on the interfacial anisotropy [56,57,79], the uniformity of the magnetic properties of the ferromagnet, and now, even the amplitude of the VCMA effect [78,80].

IV. CRYOGENIC TEMPERATURE DEPENDENCE OF THE VCMA EFFECT

Finally, the temperature dependence of the VCMA effect is characterized down to 5 K, to investigate whether the VCMA effect in STO may be related to ionic motion or oxygen vacancies. In case of an ionic, or redox VCMA effect, the temperature dependence should show an Arrhenius-law behavior and decrease with decreasing temperature.

A. VCMA measurements

From the shape of the in-plane magnetization loops [see Fig. 4(a)] and $B_{K0,K2}$ [see Fig. 4(b)], it appears that the anisotropy increases significantly with decreasing temperature (for out-of-plane magnetization loops see Supplementary Section SIV [42] and references [81–90]). For bulk cobalt, the magnetocrystalline anisotropy constants (both uniaxial K_0 and K_2) increase with decreasing temperature [91]. In Co/Pt thin films, the uniaxial anisotropy energy K_{eff} also increases with decreasing temperature [18,92,93]. This is likely due to the increase in magnetocrystalline interfacial anisotropy K_i . Here, the anisotropy field increases from 355 mT ($K_{\text{eff}} = 0.11$ mJ/m²) at room temperature to 656 mT at 5 K ($K_{\text{eff}} = 0.34$ mJ/m²).

In ALD-grown oxides, charge trapping in defects leads to an additional, temperature-dependent capacitance signal [31]. The defects are gradually deactivated as the temperature decreases and the capture and emission times become larger. So at lower temperatures, the measured capacitance (and therefore permittivity κ) is closer to the real permittivity of the ALD oxide layer [31].

The temperature dependence of the anisotropy field modulation VCB_{K0} (with B_{K2} fixed) is unmistakably different from that of the permittivity [see Fig. 4(d)]. Whereas the measured κ of STO slowly decreases with decreasing temperature, the room temperature VC $B_{K0} = 19.6 \pm 1.4$ mT/V increases to 29.9 ± 2.5 mT/V at 200 K. Between 200 and 100 K, the VC B_{K0} gradually drops to 1 ± 2.1 mT/V, effectively zero. (Below 100 K, the magnetic field range and step size of the VCMA measurement is doubled, therefore the error on the VC B_{K0} and VCMA effect appears larger; it is due to the fewer datapoints for fitting the ST model).

The VCMA effect amplitude is calculated from the VCB_{K0} amplitude using Eq. (3) with the temperature dependent magnetization $M_S(T)$ [Fig. 4(c)]. The temperature-dependent VCMA effect strength is shown in Fig. 4(d).

B. Origin of the temperature dependence

To investigate the origin of the temperature dependence, the permittivity κ of STO is measured [see Fig. 4(e)]. For

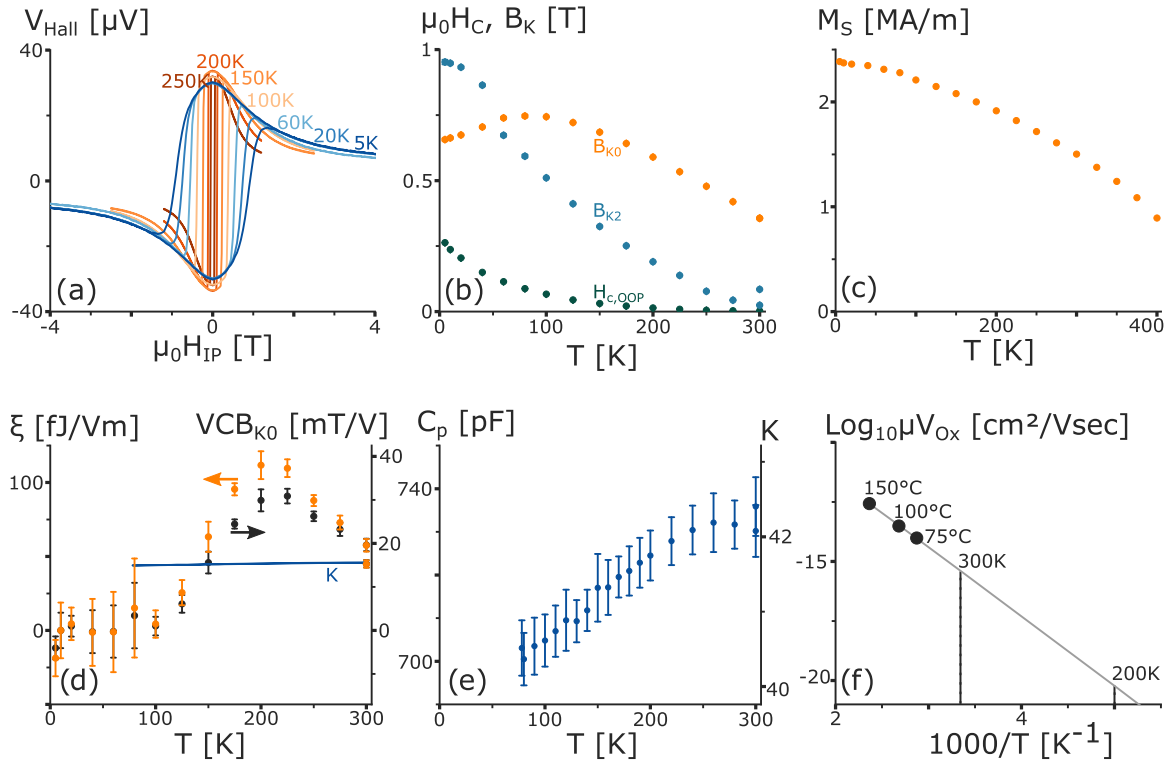


FIG. 4. The VCMA effect in STO/CoPt/Pt at cryogenic temperatures. (a) The AHE curves at different temperatures for $\theta_H = 82^\circ$. (b) The temperature dependence of the coercivity H_c , the zeroth and second order anisotropy fields $B_{K0, K2}$. (c) The temperature dependence of the magnetization M_S . (d) The amplitude of the VCMA effect ξ and the voltage control of B_{K0} as a function of temperature. The trend line of the permittivity κ is added for comparison. The discrepancy between VCB_{K0} and ξ is due to the temperature dependence of the magnetization M . (e) The capacitance of a square capacitor as a function of temperature, and corresponding permittivity κ . (f) Temperature dependence of the mobility of oxygen vacancies $\mu_{V_{Ox}}$ from Ref. [33] (dots) and Arrhenius extrapolation using Eq. (4) (line).

decreasing temperature, the permittivity decreases from 42 at 300 K to 40.5 at 78 K. This is in contrast with single-crystal STO, where κ increases from 330 at room temperature to 24 123 at 4.2 K [37] (but also strongly decreases with increasing electric field). Single crystal STO is an incipient ferroelectric [94,95]: it has a ferroelectric Curie temperature T_C very close to 0 K and is paraelectric at room temperature. In STO single crystals, the VCMA effect was reported to increase with decreasing temperature following the same trend as the permittivity [21]. However, in ALD-grown STO layers, the temperature dependence of the permittivity alone does not explain the behavior of the VCMA effect coefficient.

One potential explanation is that the VCMA effect in ALD-grown STO layers is due to the motion of oxygen vacancies or ionic species. Certainly, ionic VCMA would account for the sharp drop in the amplitude of the VCMA effect that takes place from 200 to 100 K [see Fig. 4(d)] since it is thermally activated [34,36,96]. However, the hypothesis of ionic VCMA based on oxygen vacancies cannot explain the sharp increase from room temperature down to 200 K. Indeed, the mobility of oxygen vacancies $\mu_{V_{Ox}}$ obeys the following Arrhenius law [32]:

$$\mu_{V_{Ox}} = \frac{A}{T} \exp\left(\frac{-E_0}{k_B T}\right) \quad (4)$$

where A is a constant, T is the temperature, k_B is the Boltzmann constant and E_0 is the activation energy. In our ALD

STO layers, the activation energy is around $E_0 = 0.6$ eV [33]. From Eq. (4), the mobility of oxygen vacancies should decrease with five orders of magnitude from 300 to 200 K [see Fig. 4(f)]. The VCMA effect, on the other hand, doubles in that temperature range.

The mobility of oxygen vacancies determines the kinetics of the VCMA effect rather than its strength. If the characteristic timescale of oxygen vacancy (or ion) motion is much faster than that of the measurement, a dramatic drop of the mobility may not suppress the VCMA effect. At room temperature, the characteristic timescale of oxygen vacancy motion in a 10-nm-thick STO layer at $V_{Gate} = 0.5$ V is of the order of 3000 sec (τ_{peak} calculated from reference [33]). This time-frame is just barely longer than that of the measurement, and therefore a room temperature analysis alone does not allow to exclude an ionic contribution to VCMA in these samples. (Ideally, the room temperature effect should be investigated with high-frequency measurements to distinguish between ionic and electronic VCMA.) The same ionic effect at 200 K, on the other hand, takes place within a time frame of 3×10^8 seconds or 10 years. In summary, this provides evidence that the temperature dependence of the VCMA effect in ALD-STO cannot be ascribed to an ionic effect.

Purely electronic VCMA should be interpreted in the context of the theoretical framework developed by Suzuki and Miwa [5]. Considering the interdiffused nature of the Co/Pt bilayer, both the orbital mechanism dominant in Co [44] and

the quadrupole mechanism dominant in Pt [97] are likely to play a role. The nonmonotonous temperature dependence is hence possibly due to a change in the relative strength of both contributions. In order to quantitatively understand the temperature dependence of the VCMA effect, the contribution of both the orbital and quadrupole mechanisms should be investigated, using, e.g., x-ray magnetic circular dichroism (XMCD). These measurements, combined with *ab initio* simulations would prove valuable in understanding the nature of VCMA in ALD-grown STO/Co(Pt)/Pt multilayers.

V. CONCLUSION

Three conclusions can be drawn. First, surface engineering of the STO layer is the key to a Co(Pt) magnetic layer with uniform magnetization switching. It appears that a simple IPA clean prior to deposition of the metal layers is sufficient. The IPA clean promotes the formation of a CoO_x layer at the STO/Co(Pt) interface. We propose as an explanation that the CoO_x interlayer suppresses crystalline and chemical defects, which otherwise act as domain wall pinning sites and lead to nonuniform magnetization switching. Second, in a STO/Co(Pt)/Pt stack with uniform switching, the VCMA effect has a strength between $\xi = 50$ and 75 fJ/Vm. Third, the VCMA effect strength in STO/Co(Pt)/Pt doubles as the temperature is decreased from 300 to 200 K, and then drops to zero as the temperature decreases to 100 K and below. This temperature dependence contradicts the possibility that the VCMA effect would be of ionic origin. To investigate this in more detail, characterization such as high-frequency and XMCD measurements and potentially simulations are interesting.

VI. METHODS

The samples are fabricated on Si wafers after an O₃ based clean leaving 1 nm of amorphous SiO₂. A forming gas anneal at 420 °C for 20 min is applied to passivate dangling bonds, after which 10 nm of TiN is sputter deposited. A 10-nm-thick amorphous Sr-rich ALD SrTiO₃ (STO) layer is deposited at 350 °C in an ASM Polygon 8300 reactor (the process is described in Ref. [29]). The SrTiO₃ layer is annealed at 600 °C

for 60 sec in N₂ to promote cubic (110) crystallinity. The samples are then transferred through air to a Canon Anelva PVD reactor. Before the metal deposition, the samples undergo a surface treatment discussed in Ref. [42]. Subsequently, a Co wedge with thickness ranging from 0.6 to 2.4 nm is sputter-deposited, followed by 4 nm of Pt and 5 nm of Ru. Samples are finally annealed at a temperature of 300 °C at atmospheric pressure for 10 min in N₂ ambient. TEM and energy dispersive x-ray spectroscopy (EDS) specimens are prepared using conventional ion milling and imaged in a FEI Titan at 300kV. Rutherford backscattering spectra (RBS) were obtained using a He⁺ beam with an energy of 1.523 MeV, at a scattering angle of 170° and sample tilt angle of 11°. RBS is used to measure the thickness of Co layers at different locations on 300 mm wafers, with an accuracy of 5%. Vibrating sample magnetometry (VSM) measurements were performed using a Microsense EV11 tool at room temperature on 8 × 8 mm² samples. The anomalous Hall effect measurements are performed in a home-built electrical probing tool equipped with water-cooled AML 4H2-45 magnet. The samples are affixed to a small PCB using silver paste, and attached to a vertical rod rotating in the magnetic field. The cryo VCMA measurement are performed using a physical property measurement system (PPMS) made by Quantum Design.

ACKNOWLEDGMENTS

We wish to acknowledge the support of J. Meerschaet for fruitful discussions on Rutherford Backscattering Spectrometry; W. Keijers and B. Raes for assistance with the PPMS measurements; S. Basov and M. Van Bael for SQUID measurements; H. Bender for assisting in the analysis of TEM micrographs and EDS spectra; P.J. Roussel for helping in the analysis of VCMA data; V. Afanasiev and A. Stesmans for interesting discussions on dielectrics, SrTiO₃ in particular. We acknowledge the financial support of the Fund for Scientific Research Foundation - Flanders (FWO) through Grant No. G0D5315N and the KULeuven Concerted Research Actions (GOA/14/007) and Grant No. C14/18/074 as well as the European Magnetometry Network. The authors declare no conflict of interest.

-
- [1] K. Ando, S. Fujita, J. Ito, S. Yuasa, Y. Suzuki, Y. Nakatani, T. Miyazaki, and H. Yoda, Spin-transfer torque magnetoresistive random-access memory technologies for normally off computing, *J. Appl. Phys.* **115**, 172607 (2014).
- [2] C. Grezes, F. Ebrahimi, J. Alzate, X. Cai, J. Katine, J. Langer, B. Ocker, P. Khalili Amiri, and K. Wang, Ultra-low switching energy and scaling in electric-field-controlled nanoscale magnetic tunnel junctions with high resistance-area product, *Appl. Phys. Lett.* **108**, 012403 (2016).
- [3] S. Kanai, F. Matsukura, and H. Ohno, Electric-field-induced magnetization switching in CoFeB/MgO magnetic tunnel junctions with high junction resistance, *Appl. Phys. Lett.* **108**, 192406 (2016).
- [4] T. Maruyama, Y. Shiota, T. Nozaki, K. Ohta, N. Toda, M. Mizuguchi, A. Tulapurkar, T. Shinjo, M. Shiraishi, S. Mizukami, Y. Ando, and Y. Suzuki, Large voltage-induced magnetic anisotropy change in a few atomic layers of iron, *Nat. Nanotechnol.* **4**, 158 (2009).
- [5] Y. Suzuki and S. Miwa, Magnetic anisotropy of ferromagnetic metals in low-symmetry systems, *Phys. Lett. A* **383**, 1203 (2019).
- [6] T. Nozaki, T. Yamamoto, S. Miwa, M. Tsujikawa, M. Shirai, S. Yuasa, and Y. Suzuki, Recent progress in the voltage-controlled magnetic anisotropy effect and the challenges faced in developing voltage-torque MRAM, *Micromachines* **10**, 327 (2019).
- [7] X. Li, A. Lee, S. A. Razavi, H. Wu, and K. L. Wang, Voltage-controlled magnetoelectric memory and logic devices, *MRS Bull.* **43**, 970 (2018).
- [8] P. Bruno, Tight-binding approach to the orbital magnetic moment and magnetocrystalline anisotropy of transition-metal monolayers, *Phys. Rev. B* **39**, 865 (1989).

- [9] S. Miwa, J. Fujimoto, P. Risius, K. Nawaoka, M. Goto, and Y. Suzuki, Strong bias effect on voltage-driven torque at epitaxial Fe/MgO interface, *Phys. Rev. X* **7**, 031018 (2017).
- [10] T. Nozaki, H. Arai, K. Yakushiji, S. Tamaru, H. Kubota, H. Imamura, A. Fukushima, and S. Yuasa, Magnetization switching assisted by high-frequency-voltage-induced ferromagnetic resonance, *Appl. Phys. Express* **7**, 073002 (2014).
- [11] A. Kozioł-Rachwał, T. Nozaki, K. Freindl, J. Korecki, S. Yuasa, and Y. Suzuki, Enhancement of perpendicular magnetic anisotropy and its electric field-induced change through interface engineering in Cr/Fe/MgO, *Sci. Rep.* **7**, 5993 (2017).
- [12] T. Nozaki, A. Kozioł-Rachwał, M. Tsujikawa, Y. Shiota, X. Xu, T. Ohkubo, T. Tsukahara, S. Miwa, M. Suzuki, S. Tamaru, H. Kubota, A. Fukushima, K. Hono, M. Shirai, Y. Suzuki, and S. Yuasa, Highly efficient voltage control of spin and enhanced interfacial perpendicular magnetic anisotropy in iridium-doped Fe/MgO magnetic tunnel junctions, *NPG Asia Mater.* **9**, e451 (2017).
- [13] Y. Shiota, T. Maruyama, T. Nozaki, T. Shinjo, M. Shiraishi, and Y. Suzuki, Voltage-assisted magnetization switching in ultrathin Fe₈₀Co₂₀ alloy layers, *Appl. Phys. Express* **2**, 063001 (2009).
- [14] M. Endo, S. Kanai, S. Ikeda, F. Matsukura, and H. Ohno, Electric-field effects on thickness dependent magnetic anisotropy of sputtered MgO/Co₄₀Fe₄₀B₂₀/Ta structures, *Appl. Phys. Lett.* **96**, 212503 (2010).
- [15] K. Kita, D. W. Abraham, M. J. Gajek, and D. Worledge, Electric-field-control of magnetic anisotropy of Co_{0.6}Fe_{0.2}B_{0.2}/oxide stacks using reduced voltage, *J. Appl. Phys.* **112**, 033919 (2012).
- [16] X. Li, G. Yu, H. Wu, P. Ong, K. Wong, Q. Hu, F. Ebrahimi, P. Upadhyaya, M. Akyol, and N. Kioussis, Thermally stable voltage-controlled perpendicular magnetic anisotropy in Mo/CoFeB/MgO structures, *Appl. Phys. Lett.* **107**, 142403 (2015).
- [17] D. Chien, X. Li, K. Wong, M. A. Zurbuchen, S. Robbenolt, G. Yu, S. Tolbert, N. Kioussis, P. Khalili Amiri, and K. L. Wang, Enhanced voltage-controlled magnetic anisotropy in magnetic tunnel junctions with an MgO/PZT/MgO tunnel barrier, *Appl. Phys. Lett.* **108**, 112402 (2016).
- [18] K. Yamada, H. Kakizakai, K. Shimamura, M. Kawaguchi, S. Fukami, N. Ishiwata, D. Chiba, and T. Ono, Electric field modulation of magnetic anisotropy in MgO/Co/Pt structure, *Appl. Phys. Express* **6**, 073004 (2013).
- [19] T. Kawabe, K. Yoshikawa, M. Tsujikawa, T. Tsukahara, K. Nawaoka, Y. Kotani, K. Toyoki, M. Goto, M. Suzuki, T. Nakamura, M. Shirai, Y. Suzuki, and S. Miwa, Electric-field-induced changes of magnetic moments and magnetocrystalline anisotropy in ultrathin cobalt films, *Phys. Rev. B* **96**, 220412(R) (2017).
- [20] T. Koyama and D. Chiba, Influence of the magnetization reversal mechanism on the electric field modulation of coercivity in Pt/Co structures, *Phys. Rev. B* **96**, 224409 (2017).
- [21] S. Nakazawa, A. Obinata, D. Chiba, and K. Ueno, Electric field control of magnetic anisotropy in a Co/Pt bilayer deposited on a high- κ SrTiO₃, *Appl. Phys. Lett.* **110**, 062406 (2017).
- [22] S. Kasukawa, Y. Shiota, T. Moriyama, and T. Ono, Evaluation of electric field effect on interface magnetic properties by propagating spin wave in Pt/Co/MgO structures, *Jpn. J. Appl. Phys.* **57**, 080309 (2018).
- [23] F. Tan, G. Lim, T. Jin, H. Liu, F. Poh, and W. Lew, Electric field control on single and double Pt/Co heterostructure for enhanced thermal stability, *J. Magn. Magn. Mater.* **490**, 165448 (2019).
- [24] X. Li, K. Fitzell, D. Wu, C. T. Karaba, A. Buditama, G. Yu, K. L. Wong, N. Altieri, C. Grezes, and N. Kioussis, Enhancement of voltage-controlled magnetic anisotropy through precise control of Mg insertion thickness at CoFeB/MgO interface, *Appl. Phys. Lett.* **110**, 052401 (2017).
- [25] C.-G. Duan, J. P. Velev, R. F. Sabirianov, Z. Zhu, J. Chu, S. S. Jaswal, and E. Y. Tsybmal, Surface Magnetoelectric Effect in Ferromagnetic Metal Films, *Phys. Rev. Lett.* **101**, 137201 (2008).
- [26] C.-G. Duan, J. P. Velev, R. F. Sabirianov, W.-N. Mei, S. S. Jaswal, and E. Y. Tsybmal, Tailoring magnetic anisotropy at the ferromagnetic/ferroelectric interface, *Appl. Phys. Lett.* **92**, 122905 (2008).
- [27] M. K. Niranjana, C.-G. Duan, S. S. Jaswal, and E. Y. Tsybmal, Electric field effect on magnetization at the Fe/MgO (001) interface, *Appl. Phys. Lett.* **96**, 222504 (2010).
- [28] T. Hirai, T. Koyama, and D. Chiba, Control of magnetism by electrical charge doping or redox reactions in a surface-oxidized Co thin film with a solid-state capacitor structure, *Appl. Phys. Lett.* **112**, 122408 (2018).
- [29] M. Popovici, S. Van Elshocht, N. Menou, J. Swerts, D. Pierreux, A. Delabie, B. Brijs, T. Conard, K. Opsomer, J. Maes, D. Wouters, and J. Kittl, Atomic layer deposition of strontium titanate films using Sr(^{#2}#1Cp)₂ and Ti (OMe)₄, *J. Electrochem. Soc.* **157**, G1 (2010).
- [30] M. Popovici, B. Kaczer, V. V. Afanas'ev, G. Sereni, L. Larcher, A. Redolfi, S. Van Elshocht, and M. Jurczak, Low leakage stoichiometric SrTiO₃ dielectric for advanced metal/insulator/metal capacitors, *Phys. Statu Solidi (RRL)-Rapid Research Letters* **10**, 420 (2016).
- [31] A. Padovani, B. Kaczer, M. Pešić, A. Belmonte, M. Popovici, L. Nyns, D. Linten, V. V. Afanas'ev, I. Shlyakhov, Y. Lee, H. Park, and L. Larcher, A sensitivity map-based approach to profile defects in MIM capacitors from I-V, C-V and G-V measurements, *IEEE Trans. Electron Devices* **66**, 1892 (2019).
- [32] S. Zafar, R. E. Jones, B. Jiang, B. White, P. Chu, D. Taylor, and S. Gillespie, Oxygen vacancy mobility determined from current measurements in thin Ba_{0.5}Sr_{0.5}Ti₃ films, *Appl. Phys. Lett.* **73**, 175 (1998).
- [33] M.-S. Kim, B. Kaczer, S. Starschich, M. Popovici, J. Swerts, O. Richard, K. Tomida, C. Vrancken, S. Van Elshocht, I. Debusschere, L. Altimime, and J. Kittl, Understanding of trap-assisted tunneling current-assisted by oxygen vacancies in RuO_x/SrTiO₃/TiN MIM capacitor for the DRAM application, in *2012 4th IEEE International Memory Workshop (IEEE, 2012)* pp. 1–4.
- [34] U. Bauer, L. Yao, A. J. Tan, P. Agrawal, S. Emori, H. L. Tuller, S. Van Dijken, and G. S. Beach, Magneto-ionic control of interfacial magnetism, *Nat. Mater.* **14**, 174 (2015).
- [35] L. Baldrati, A. Tan, M. Mann, R. Bertacco, and G. Beach, Magneto-ionic effect in CoFeB thin films with in-plane and perpendicular-to-plane magnetic anisotropy, *Appl. Phys. Lett.* **110**, 012404 (2017).
- [36] C. Bi, Y. Liu, T. Newhouse-Illige, M. Xu, M. Rosales, J. W. Freeland, O. Mryasov, S. Zhang, S. G. E. te Velthuis, and W. G. Wang, Reversible Control of Co Magnetism by Voltage-Induced Oxidation, *Phys. Rev. Lett.* **113**, 267202 (2014).

- [37] R. Neville, B. Hoeneisen, and C. Mead, Permittivity of strontium titanate, *J. Appl. Phys.* **43**, 2124 (1972).
- [38] Y. Hibino, T. Koyama, A. Obinata, T. Hirai, S. Ota, K. Miwa, S. Ono, F. Matsukura, H. Ohno, and D. Chiba, Peculiar temperature dependence of electric-field effect on magnetic anisotropy in Co/Pd/MgO system, *Appl. Phys. Lett.* **109**, 082403 (2016).
- [39] Y. Hayashi, Y. Hibino, F. Matsukura, K. Miwa, S. Ono, T. Hirai, T. Koyama, H. Ohno, and D. Chiba, Electric-field effect on magnetic anisotropy in Pt/Co/Pd/MgO structures deposited on GaAs and Si substrates, *Appl. Phys. Express* **11**, 013003 (2018).
- [40] B. F. Vermeulen, J. Wu, J. Swerts, S. Couet, D. Linten, I. P. Radu, K. Temst, G. Rampelberg, C. Detavernier, G. Groeseneken, and K. Martens, Perpendicular magnetic anisotropy of Co/Pt bilayers on ALD HfO₂, *J. Appl. Phys.* **120**, 163903 (2016).
- [41] B. F. Vermeulen, J. Wu, J. Swerts, S. Couet, I. P. Radu, G. Groeseneken, C. Detavernier, J. K. Jochum, M. Van Bael, K. Temst, A. Shukla, S. Miwa, Y. Suzuki, and K. Martens, Perpendicular magnetic anisotropy of CoFeB/Ta bilayers on ALD HfO₂, *AIP Advances* **7**, 055933 (2017).
- [42] See Supplemental Material at <http://link.aps.org/supplemental/10.1103/PhysRevMaterials.4.114415> for: the materials stack, STO aging in air and surface treatments; VCMA in the ion milled + annealed sample; a discussion of the reason why the Sucksmith-Thompson model is used for VCMA quantification; a discussion of out-of-plane $\mu_0 H$ AHE measurements at cryo temperatures.
- [43] B. F. Vermeulen, F. Ciubotaru, M. I. Popovici, J. Swerts, S. Couet, I. P. Radu, A. Stancu, K. Temst, G. Groeseneken, C. Adelmann, and K. M. Martens, Ferroelectric control of magnetism in ultrathin HfO₂/Co/Pt layers, *ACS Appl. Mater. Interfaces* **11**, 34385 (2019).
- [44] P. Bruno, Dipolar magnetic surface anisotropy in ferromagnetic thin films with interfacial roughness, *J. Appl. Phys.* **64**, 3153 (1988).
- [45] G. D. Chaves-O'Flynn, G. Wolf, J. Z. Sun, and A. D. Kent, Thermal stability of magnetic states in circular thin-film nanomagnets with large perpendicular magnetic anisotropy, *Phys. Rev. Appl.* **4**, 024010 (2015).
- [46] E. C. Stoner and E. Wohlfarth, A mechanism of magnetic hysteresis in heterogeneous alloys, *Philos. Trans. R. Soc., A* **240**, 599 (1948).
- [47] J. Livingston, A review of coercivity mechanisms, *J. Appl. Phys.* **52**, 2544 (1981).
- [48] E. Filatova, I. Kozhevnikov, A. Sokolov, A. Konashuk, F. Schaefer, M. Popovici, and V. Afanas'ev, Application of soft X-ray reflectometry for analysis of underlayer influence on structure of atomic-layer deposited SrTi_xO_y films, *J. Electron Spectrosc. Relat. Phenom.* **196**, 110 (2014).
- [49] F. Voigts, C. Argirusis, and W. Maus-Friedrichs, The interaction of CO₂ and CO with Fe-doped SrTiO₃ (100) surfaces, *Surf. Interface Anal.* **44**, 301 (2012).
- [50] N. Brookes, G. Thornton, and F. Quinn, SrTiO₃ (100) step sites as catalytic centers for H₂O dissociation, *Solid State Commun.* **64**, 383 (1987).
- [51] J.-C. Dupin, D. Gonbeau, P. Vinatier, and A. Levasseur, Systematic XPS studies of metal oxides, hydroxides and peroxides, *Phys. Chem. Chem. Phys.* **2**, 1319 (2000).
- [52] A. Amri, X. Duan, C.-Y. Yin, Z.-T. Jiang, M. M. Rahman, and T. Pryor, Solar absorptance of copper-cobalt oxide thin film coatings with nano-size, grain-like morphology: Optimization and synchrotron radiation XPS studies, *Appl. Surf. Sci.* **275**, 127 (2013).
- [53] M. C. Biesinger, B. P. Payne, A. P. Grosvenor, L. W. Lau, A. R. Gerson, and R. S. C. Smart, Resolving surface chemical states in XPS analysis of first row transition metals, oxides and hydroxides: Cr, Mn, Fe, Co and Ni, *Appl. Surf. Sci.* **257**, 2717 (2011).
- [54] A. Manchon, S. Pizzini, J. Vogel, V. Uhlir, L. Lombard, C. Ducruet, S. Auffret, B. Rodmacq, B. Dieny, M. Hochstrasser, and G. Panaccione, X-ray analysis of the magnetic influence of oxygen in Pt/Co/AlO_x trilayers, *J. Appl. Phys.* **103**, 07A912 (2008).
- [55] C. L. Canedy, X. W. Li, and G. Xiao, Large magnetic moment enhancement and extraordinary Hall effect in Co/Pt superlattices, *Phys. Rev. B* **62**, 508 (2000).
- [56] H. X. Yang, M. Chshiev, B. Dieny, J. H. Lee, A. Manchon, and K. H. Shin, First-principles investigation of the very large perpendicular magnetic anisotropy at Fe|MgO and Co|MgO interfaces, *Phys. Rev. B* **84**, 054401 (2011).
- [57] B. Rodmacq, S. Auffret, B. Dieny, S. Monso, and P. Boyer, Crossovers from in-plane to perpendicular anisotropy in magnetic tunnel junctions as a function of the barrier degree of oxidation, *J. Appl. Phys.* **93**, 7513 (2003).
- [58] A. Manchon, C. Ducruet, L. Lombard, S. Auffret, B. Rodmacq, B. Dieny, S. Pizzini, J. Vogel, V. Uhlir, M. Hochstrasser, and G. Panaccione, Analysis of oxygen induced anisotropy crossover in Pt/Co/MO_x trilayers, *J. Appl. Phys.* **104**, 043914 (2008).
- [59] M. Johnson, P. Bloemen, F. Den Broeder, and J. De Vries, Magnetic anisotropy in metallic multilayers, *Rep. Prog. Phys.* **59**, 1409 (1996).
- [60] F. Den Broeder, W. Hoving, and P. Bloemen, Magnetic anisotropy of multilayers, *J. Magn. Magn. Mater.* **93**, 562 (1991).
- [61] S. Y. Huang, X. Fan, D. Qu, Y. P. Chen, W. G. Wang, J. Wu, T. Y. Chen, J. Q. Xiao, and C. L. Chien, Transport Magnetic Proximity Effects in Platinum, *Phys. Rev. Lett.* **109**, 107204 (2012).
- [62] Y. Hibino, T. Koyama, A. Obinata, K. Miwa, S. Ono, and D. Chiba, Electric field modulation of magnetic anisotropy in perpendicularly magnetized Pt/Co structure with a Pd top layer, *Appl. Phys. Express* **8**, 113002 (2015).
- [63] Y. Shiota, S. Murakami, F. Bonell, T. Nozaki, T. Shinjo, and Y. Suzuki, Quantitative evaluation of voltage-induced magnetic anisotropy change by magnetoresistance measurement, *Appl. Phys. Express* **4**, 043005 (2011).
- [64] Y.-C. Lau, P. Sheng, S. Mitani, D. Chiba, and M. Hayashi, Electric field modulation of the non-linear areal magnetic anisotropy energy, *Appl. Phys. Lett.* **110**, 022405 (2017).
- [65] K.-W. Park, J.-Y. Park, S.-h. C. Baek, D.-H. Kim, S.-M. Seo, S.-W. Chung, and B.-G. Park, Electric field control of magnetic anisotropy in the easy cone state of Ta/Pt/CoFeB/MgO structures, *Appl. Phys. Lett.* **109**, 012405 (2016).
- [66] F. Xue, N. Sato, C. Bi, J. Hu, J. He, and S. X. Wang, Large voltage control of magnetic anisotropy in CoFeB/MgO/OX structures at room temperature, *APL Mater.* **7**, 101112 (2019).
- [67] K. Garelo, I. M. Miron, C. O. Avci, F. Freimuth, Y. Mokrousov, S. Blügel, S. Auffret, O. Boulle, G. Gaudin, and P. Gambardella, Symmetry and magnitude of spin-orbit torques in ferromagnetic heterostructures, *Nat. Nanotechnol.* **8**, 587 (2013).
- [68] J. H. van Vleck, On the anisotropy of cubic ferromagnetic crystals, *Phys. Rev.* **52**, 1178 (1937).

- [69] B. Heinrich, T. Monchesky, and R. Urban, Role of interfaces in higher order angular terms of magnetic anisotropies: Ultrathin film structures, *J. Magn. Magn. Mater.* **236**, 339 (2001).
- [70] F. Porrati, W. Wulfhekel, and J. Kirschner, An analytical model for ultrathin films with spatially varying magnetic anisotropies, *J. Magn. Magn. Mater.* **270**, 22 (2004).
- [71] J. B. Mohammadi, K. Cole, T. Mewes, and C. K. A. Mewes, Inhomogeneous perpendicular magnetic anisotropy as a source of higher-order quasistatic and dynamic anisotropies, *Phys. Rev. B* **97**, 014434 (2018).
- [72] W. Sucksmith and J. E. Thompson, The magnetic anisotropy of cobalt, *Proc. R. Soc. London. Series A: Math. Phys. Sci.* **225**, 362 (1954).
- [73] A. Sugihara, A. Spiesser, T. Nozaki, H. Kubota, H. Imamura, A. Fukushima, K. Yakushiji, and S. Yuasa, Temperature dependence of higher-order magnetic anisotropy constants and voltage-controlled magnetic anisotropy effect in a Cr/Fe/MgO junction, *Jpn. J. Appl. Phys.* **59**, 010901 (2019).
- [74] G. Yu, Z. Wang, M. Abolfath-Beygi, C. He, X. Li, K. L. Wong, P. Nordeen, H. Wu, G. P. Carman, X. Han, I. A. Alhomoudi, P. Khalili Amiri, and K. L. Wang, Strain-induced modulation of perpendicular magnetic anisotropy in Ta/CoFeB/MgO structures investigated by ferromagnetic resonance, *Appl. Phys. Lett.* **106**, 072402 (2015).
- [75] A. Okada, S. Kanai, S. Fukami, H. Sato, and H. Ohno, Electric-field effect on the easy cone angle of the easy-cone state in CoFeB/MgO investigated by ferromagnetic resonance, *Appl. Phys. Lett.* **112**, 172402 (2018).
- [76] S. Kanai, M. Gajek, D. Worledge, F. Matsukura, and H. Ohno, Electric field-induced ferromagnetic resonance in a CoFeB/MgO magnetic tunnel junction under dc bias voltages, *Appl. Phys. Lett.* **105**, 242409 (2014).
- [77] A. Okada, S. Kanai, M. Yamanouchi, S. Ikeda, F. Matsukura, and H. Ohno, Electric-field effects on magnetic anisotropy and damping constant in Ta/CoFeB/MgO investigated by ferromagnetic resonance, *Appl. Phys. Lett.* **105**, 052415 (2014).
- [78] J. Shiogai, T. Ohashi, T. Yang, M. Kohda, T. Seki, K. Takanashi, and J. Nitta, Enhancement of electric field modulation of coercivity in Pt/Co/Al-O structures by tuning Co surface oxidation, *J. Phys. D* **49**, 03LT01 (2015).
- [79] A. Manchon, S. Pizzini, J. Vogel, V. Uhlř, L. Lombard, C. Ducruet, S. Auffret, B. Rodmacq, B. Dieny, M. Hochstrasser, and G. Panaccione, X-ray analysis of oxygen-induced perpendicular magnetic anisotropy in Pt/Co/AlO_x trilayers, *J. Magn. Magn. Mater.* **320**, 1889 (2008).
- [80] T. Hirai, T. Koyama, A. Obinata, Y. Hibino, K. Miwa, S. Ono, M. Kohda, and D. Chiba, Control of magnetic anisotropy in Pt/Co system using ionic liquid gating, *Appl. Phys. Express* **9**, 063007 (2016).
- [81] R. Karplus and J. Luttinger, Hall effect in ferromagnetics, *Phys. Rev.* **95**, 1154 (1954).
- [82] L. Berger, Side-jump mechanism for the Hall effect of ferromagnets, *Phys. Rev. B* **2**, 4559 (1970).
- [83] J. Smit, The spontaneous Hall effect in ferromagnetics II, *Physica* **24**, 39 (1958).
- [84] S. Zhang, J. Teng, J. Zhang, Y. Liu, J. Li, G. Yu, and S. Wang, Large enhancement of the anomalous Hall effect in Co/Pt multilayers sandwiched by MgO layers, *Appl. Phys. Lett.* **97**, 222504 (2010).
- [85] J. Kötzer and W. Gil, Anomalous hall resistivity of cobalt films: Evidence for the intrinsic spin-orbit effect, *Phys. Rev. B* **72**, 060412(R) (2005).
- [86] D. Hou, Y. Li, D. Wei, D. Tian, L. Wu, and X. Jin, The anomalous Hall effect in epitaxial face-centered-cubic cobalt films, *J. Phys.: Condens. Matter* **24**, 482001 (2012).
- [87] Y. Wang, F. Liu, C. Cao, C. Zhou, G. Chai, and C. Jiang, Ionic-liquid gating controls anomalous hall resistivity of Co/Pt perpendicular magnetic anisotropy films, *J. Magn. Magn. Mater.* **491**, 165626 (2019).
- [88] S.-L. Jiang, X. Chen, X.-J. Li, K. Yang, J.-Y. Zhang, G. Yang, Y.-W. Liu, J.-H. Lu, D.-W. Wang, J. Teng, and G.-H. Yu, Anomalous Hall effect engineering via interface modification in Co/Pt multilayers, *Appl. Phys. Lett.* **107**, 112404 (2015).
- [89] J. Sugiyama, H. Nozaki, J. H. Brewer, E. J. Ansaldo, T. Takami, H. Ikuta, and U. Mizutani, Appearance of a two-dimensional antiferromagnetic order in quasi-one-dimensional cobalt oxides, *Phys. Rev. B* **72**, 064418 (2005).
- [90] F. J. Ferraro, Ph.D. thesis, Université Grenoble Alpes, 2015.
- [91] B. D. Cullity and C. D. Graham, *Introduction to Magnetic Materials* (Wiley, Piscataway, NJ, USA, 2011).
- [92] T. Nozaki, M. Oida, T. Ashida, N. Shimomura, and M. Sahashi, Temperature-Dependent Perpendicular Magnetic Anisotropy of Co-Pt on Cr₂O₃ antiferromagnetic oxide, *Appl. Phys. Lett.* **103**, 242418 (2013).
- [93] H. Garad, F. Fettar, F. Gay, Y. Joly, S. Auffret, B. Rodmacq, B. Dieny, and L. Ortega, Temperature Variation of Magnetic Anisotropy in Pt/Co/AlO_x Trilayers, *Phys. Rev. Appl.* **7**, 034023 (2017).
- [94] J. Haeni, P. Irvin, W. Chang, R. Uecker, P. Reiche, Y. Li, S. Choudhury, W. Tian, H. ME, B. Craigo, A. Tagantsev, X. Pan, S. SK, L. Chen, S. Kierchoefer, J. Levy, and D. Schlom, Room-temperature ferroelectricity in strained SrTiO₃, *Nature (London)* **430**, 758 (2004).
- [95] S. Schmidt, J. Lu, S. P. Keane, L. D. Bregante, D. O. Klenov, and S. Stemmer, Microstructure and dielectric properties of textured SrTiO₃ thin films, *J. Am. Ceram. Soc.* **88**, 789 (2005).
- [96] S. Miwa, M. Suzuki, M. Tsujikawa, T. Nozaki, T. Nakamura, M. Shirai, S. Yuasa, and Y. Suzuki, Perpendicular magnetic anisotropy and its electric-field-induced change at metal-dielectric interfaces, *J. Phys. D* **52**, 063001 (2018).
- [97] S. Miwa, M. Suzuki, M. Tsujikawa, K. Matsuda, T. Nozaki, K. Tanaka, T. Tsukahara, K. Nawaoka, M. Goto, Y. Kotani, T. Ohkubo, F. Bonell, E. Tamura, K. Hono, T. Nakamura, M. Shirai, S. Yuasa, and Y. Suzuki, Voltage controlled interfacial magnetism through platinum orbits, *Nat. Commun.* **8**, 15848 (2017).